Effects of periodicity on flow and dispersion through closely packed fixed beds of spheres

A. M. Reynolds*
Silsoe Research Institute, Wrest Park, Silsoe, Bedford, MK45 4HS, United Kingdom
(Received 10 April 2001; revised manuscript received 4 October 2001; published 23 January 2002)

A lattice-Boltzmann formulation is used to investigate the effects of ''periodicity'' (geometry) on fluid flow and tracer-particle dispersion through fixed beds of spheres comprising of closely packed layers. In the ''period-1'' arrangement, spheres in the adjacent layers contact at their poles while the ''period-2'' and ''period-3'' arrangements correspond to hexagonal and faced-centered cubic close packing. For all three packing arrangements, there is a transition with increasing Reynolds number from a power law to a log-normal distribution of kinetic energies and, velocity and vorticity become more closely aligned giving rise to helical tracer-particle trajectories. It is suggested that these flow characteristics, unlike the stability of flow and the distribution of helicity, are largely insensitive to geometry, even when the geometry creates direct channels through the pack bed orientated along the gradient in applied pressure. For steady flows and strongly turbulent flows, such channels are predicted to provide direct routes for dispersion through a packed bed, while for weakly turbulent flows they influence dispersion primarily by destabilizing the flow and thereby promoting dispersion throughout a bed. The dispersion of tracer-particles released from a source located on or close to a ''stagnation streamline'' is predicted to be faster than ballistic in the near field and the transition to long-time Fickian diffusion is predicted to be distinguished by a regime of subdiffusion.

DOI: 10.1103/PhysRevE.65.026308 PACS number(s): 47.55.Mh, 47.27.−i, 87.15.−v

I. INTRODUCTION

In this paper, the effects of periodicity on fluid flow and tracer-particle dispersion through fixed beds of spheres comprising of closely packed layers is examined in numerical studies using a lattice Boltzmann formulation. In the ''period 1'' arrangement, spheres in adjacent layers contact at their poles (i.e., the unit cell is an equilateral prism) while the ''period 2'' and ''period 3'' arrangements correspond to hexagonal close packing (hcp) and face-centered close packing (fcc). The period-1 and -2 arrangements are distinctly different from the period-3 arrangement in that they have direct channels for flow and dispersion orientated along a principal axis [001] which in most practical situations will be the orientation of a gradient in applied pressure and the orientation adopted here. For the period-3 arrangement, the [111] direction is a more natural orientation for the gradient in applied pressure [1].

Some indication of the importance of geometry comes from the numerical studies of Reynolds, Reavell, and Harral *et al.* [1] and Hill and Koch [2,3] who in their investigations of flow through a fixed close-packed bed of spheres in a fcc arrangement, observed the same sequence of flow transitions but found that critical Reynolds numbers were dependent upon the orientation of the gradient in applied pressure (i.e., upon geometry). More strikingly, Ladd and Koch [4] in their numerical investigation of flow through two-dimensional arrays of cylinders found that both the critical Reynolds and the nature of the transitions are dependent upon the orientation of the gradient in applied pressure.

Of particular interest will be the effects of ''periodicity'' upon distributions of kinetic energy, vorticity, and the alignment of vorticity and velocity. It will be shown later that these distributions play a key role in determining transport processes. Transport processes in fixed beds and porous media tend to be ballistic at sufficiently short times and Fickian at sufficiently large times [5]; the notable exceptions being gaseous dispersion driven by adiabatic expansion [6] and dispersion in structures having a fractal dimension. This leaves the nature of dispersion at intermediate times open to speculation; despite it obvious importance to a proper understanding of the transport processes and model parametrization. This is particularly true of turbulent flows that are not amendable to analytic analysis but which are nevertheless of considerable practical importance. It can be anticipated, on the basis of a generalization of rapid distortion theory [7,8], that the presence of stagnation points in a flow leads to anomalously large dispersion at intermediate times for sources in the vicinity of the ''stagnation streamline.'' It is even conceivable, given the expected profusion of singular points in flows through packed beds, that there is anomalous power-law dispersion at intermediate times, analogous to the superdiffusive characteristic of tracer particles in simulated two-dimensional turbulence [9] and the dispersion of drifters in the ocean [10–13] that is closely associated with the presence of hyperbolic and elliptic points in such flows [9]. In this paper, the nature of intermediate-time dispersion through fixed beds is investigated.

The remainder of this paper is organized as follows. The next section contains a brief description of the lattice-Boltzmann formulation and the numerical simulation of tracer gas dispersion. Flow and dispersion characteristics are then described in Sec. III. Conclusions are drawn in the final section.

II. NUMERICAL SIMULATIONS

A. Lattice-Boltzmann simulations

This section provides a brief description of the lattice-Boltzmann method (LBM) and its application to the simula-

*Fax: +44(0)1525860156;
email address: andy.reynolds@bbsrc.ac.uk

tion of flows through close-packed beds of spheres. More detailed descriptions of the particular LB formulation adopted, commonly denoted by D_3Q_{15}, can be found in Qian, d'Humieres, and Lallemand [14] and Chen and Doolen [15].

In the LBM, a discrete analogue of the linearized Boltzmann equation

$$f_1(\mathbf{x}+\mathbf{c}_i,t+1)-f_1(\mathbf{x},\ t)=-\frac{1}{\tau}[f_1(\mathbf{x},\ t)-f_1^{\mathrm{eq}}(\mathbf{x},\ t)] \tag{1}$$

is solved for the number density of molecules at node $\mathbf{x}$ at time t, $f_1(\mathbf{x}, t)$, of a gas of ''fictitious'' molecules that translate from node to node on a cubic lattice with a discrete set of velocities, c_i. In the present model, there are six velocities of speed one corresponding to the (100) directions, eight velocities of speed $\sqrt{3}$ corresponding to the (111) directions and one ''rest'' particle of speed zero. The distribution $f_1(\mathbf{x}, t)$ is related to the fluid density ρ and the momentum density $\mathbf{j}=\rho\mathbf{u}$, by

$$\rho=\sum_i f_1, \quad \mathbf{j}=\sum_i f_1 c_u, \tag{2}$$

and the nondimensional kinematic viscosity of the fluid ν is related to the nondimensional relaxation time τ by $\nu=(2\tau-1)/6$. Appropriate forms for equilibrium distributions, $f_1^{\mathrm{eq}}(\mathbf{x}, t)$, are taken from Qian, d'Humieres, and Lallemand [14]

$$f_1^{\mathrm{eq}}=t_1\rho\left(1+\frac{1}{c_s^2}(\mathbf{c}_i\cdot\mathbf{u})+\frac{1}{2c_s^2}(\mathbf{c}_i\cdot\mathbf{u})^2-\frac{1}{2c_s^2}u^2\right), \tag{3}$$

where $t_1=2/9$ for rest particles, 1/9 for particles with speed 1 and 1/72 for particles with speed $\sqrt{3}$. The speed of sound $\mathbf{c}_s=1/\sqrt{3}$.

Each solid sphere is defined by a spherical surface which cuts some of the links between the lattice nodes. The fictitious gas molecules moving along these links were reflected so that, in a single time step, they return to the lattice nodes from where they came with an opposite velocity. As a result, a no-slip velocity condition is imposed midway along the link. It is this easy implementation of the no-slip velocity condition by the ''bounce-back boundary scheme'' which makes the LBM ideal for simulating fluid flows in complicated geometries. The bounce-back scheme is, however, only first order in numerical accuracy at the boundary [16] and so degrades the LBM, which for the interior nodes is second order in numerical accuracy. Bounce-back schemes that are second-order accurate have been proposed [17] but cannot be readily implemented for complicated geometries. For this reason, they are not employed here. It should also be noted that this paper predates the appearance of the paper by Verberg and Ladd [18] which describes a LBM approach that is second-order accurate at the boundary.

The discrete representation of the spheres becomes more spherical with increasing sphere-radius-to-node spacing ratio. However, the size of the lattice required to obtain accurate results is primarily controlled by the need to resolve flow within the voids between neighboring spheres. The results of numerical simulations indicated that when void cross-sectional areas (approximately triangular in shape) contained more than about $1/2\times25\times25$ nodes, grid independent results (errors of less than 5%) were obtained for flows with $\mathrm{Re}<400$ through the period-1 arrangement and for flows with $\mathrm{Re}<120$ for the period-2 arrangement. This was achieved by having computational cells containing $70\times100\times100$ nodes and $60\times104\times98$ nodes for the period-1 and period-2 arrangements, respectively. The maximum mean velocity was less than the speed of sound so ensuring incompressible fluid dynamics. The ability to simulate directly flows within the period-1 arrangement with relatively large Reynolds numbers is a simple consequence of the greater stability of nonturbulent flows within such structures (see Sec. III A). Flows with larger Reynolds numbers were simulated using the LBM was used in conjunction with a subgrid model [19], with a Smagorinky constant, $C_s=0.1$.

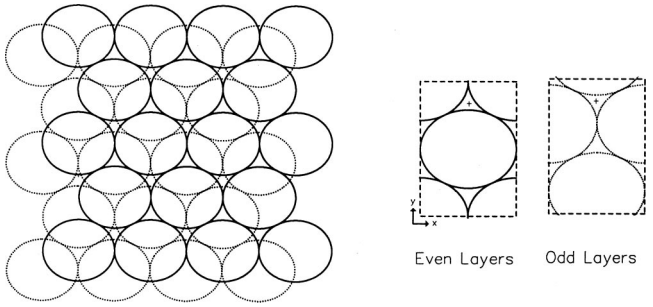

FIG. 1. Locations of spheres in alternate layers of a hexagonal close arrangement (left). Also shown (right) are the locations of the spheres within the computational cell, that comprises of two ''even'' layers and an ''odd'' layer. Periodic boundary conditions are applied at the top, bottom, and sides (dashed lines) of the cell. The location of an open channel through the cell and aligned with the direction of the applied pressure (the z direction) is indicated (+). The computational cell for the period-1 arrangement of spheres comprises of two ''even'' layers.

The computational cells utilized in the numerical modeling are indicated in Fig. 1. Periodic boundary conditions were applied at the edges of these cells, thereby facilitating the simulation of flows through packed beds of infinite extent. The gradient in applied pressure was assumed not to vary significantly across the computational cells so that its effects could be modeled accurately by a constant body-force $\mathbf{F}=(0,0,F)$. This was implemented by calculating the equilibrium distribution functions with an altered fluid velocity $\mathbf{u}+\tau\mathbf{F}/\rho$ rather than with the actual fluid velocity $\mathbf{u}$ [20].

For the period-1 and -2 arrangements, the initial value problem was solved in which the fluid velocity was zero throughout the domain and a body force was applied at time $t=0$. The chaotic (turbulent) solutions to the LBM were taken to be converged when both the mean flow and the velocity variance varied by less than 1% during the last 25% of the run. Typically, 600 000 time steps were required. A detailed description of the computations for the period-3 arrangement can be found in Reynolds, Reavell, and Harral [1].

B. Simulation of particle trajectories

There are two possible approaches to the modeling of particle dispersion. In the Eulerian approach, a diffusion-advection equation for the time evolution of a scalar is solved while in the Lagrangian approach, mean concentrations of a scalar are calculated by ensemble averaging over the simulated independent tracer-particle trajectories. In this paper the Lagrangian approach is adopted because: the boundary conditions do not need to be specified *a prori* in an *ad hoc* fashion; the approach does not introduce numerical diffusion and; because it can be readily extended to ''heavy'' particles.

The trajectories of tracer-particles $(\mathbf{x}_f,\ \mathbf{u}_f)$ were simulated by numerical integration of the tracer advection equation

$$\frac{d\mathbf{x}_f}{dt}=\mathbf{u}_1(\mathbf{x}_f,\ t), \tag{4}$$

where to filter out the effects of the staggered momentum, inherent in the solution to the D_3Q_{15} model [21], the particle velocity $\mathbf{u}_f$, is taken to be the local fluid velocity, temporal averaged over two successive iterations of the lattice-Boltzmann model. This quantity is known only at the nodes of the computational grid and at discrete times. An approximation to this quantity at the particle location at time t was obtained by linear interpolation from the grid nodes to the particle location and from the solutions for times t' and $t'+1$ to time t where $t'\leqslant t<t'+1$.

Close to the solid boundaries the spatial resolution of the grid is not sufficient, nor can it ever be, for an accurate determination of particle trajectories. These inaccuracies, which are compounded by the interpolation, can result in the nonphysical deposition of some tracer particles. To overcome this difficulty, the flow at the boundary nodes, which is predicted to vanish, was given a small normal outward component. The magnitude of this normal component was taken to be constant throughout the flow domain and equal to the smallest value which prevented all nonphysical deposition. This was typically two or more orders of magnitude less than the magnitude of the velocity at the nearest node within the flow. The simulated trajectories of tracer particles were found to be insensitive to a tenfold increase in the value of the outward velocity component.

III. PREDICTED FLOW AND DISPERSION CHARACTERISTICS

A. Sequence of transitions

Here, as throughout, Reynolds numbers Re and Re′ are based upon the radius of a sphere, the magnitude of the volumetrically and temporally averaged fluid velocity within the voids and the root-mean-square (rms) of the magnitude of the volumetrically averaged fluid velocity. With increasing Re, flows through the period-1 and period-2 arrangements of spheres underwent a series a transitions from steady to time periodic to quasiperiodic before eventually become chaotic (turbulent) with frequency spectra exhibiting inertia subrange scaling, i.e., $S(\omega)\sim\omega^{-5/3}$ over a narrow range of frequencies. The same sequence of transitions, but with different critical Reynolds number, has also be found for the period-3 arrangement [1–3] but in stark contrast with the results of numerical simulations using the LBM for two-dimensional flows through periodic arrangements of cylinders [4], there was no indication of their being any period-multiplying transitions. Of the three closely packed arrangements, the period-1 (the nonclosed-packed) arrangement is the most stable, with steady flows persisting at Re >100, while the period-2 arrangement is the least stable becoming chaotic at Re$\approx$19.8 and having the largest ratios of Re′/Re. Characteristics of these flows and the nature of the flow transitions are further examined in Secs. III B and III C.

B. Distributions of turbulent kinetic energy

A natural quantity to statistically characterize the fluid flow associated with each node in the computational grid is the kinetic energy, $k=1/2\rho\mathbf{u}\cdot\mathbf{u}$. Figure 2 shows that the distributions of normalized kinetic-energy $E=k/k_{\max}$ for the steady and chaotic flows with Re$\ll$1 and Re$\approx$19.8 through the period-2 arrangement. It is seen that for the steady flow, the distribution $n(E)$ of E follows a power law over roughly two orders of magnitude, while for the chaotic flow, it has a log-normal distribution over roughly three orders of magnitude in analogy with the log-binomial distribution for the local currents found in the corresponding random resistor network [22,23]. Similar transitions with increasing Reynolds number from a power-law to a log-normal distribution of turbulent kinetic energies have been reported for the period-3 arrangement and were also found for the period-1 arrangement. Andrade *et al.* [24] suggested that such a power-law distribution indicates that the local kinetic energy is sensitive to the geometry of the pore structure. Consequently, when the flow is steady, the ''stagnant'' zones play a significant role in determining transport through the packed bed, in contrast with the dangling ends for the analogous electrical transport problem [22,23]. A transition from a power-law to a log-normal distribution of kinetic energies has also been predicted to occur for flows through the period-3 arrangement of spheres [1].

Several factors may contribute to the dissimilarities between the scaling of the steady and turbulent flows. At low values of Re, there is a tendency for the fluid at the local void scale to preserve the parabolic shape of the velocity profiles even when the fluid is confined to very tortuous pathways. At high values of Re, however, the irregular geometry is very effective in producing sudden and dramatic changes in the directions and magnitudes of the fluid velocities, thus distorting their parabolic profile at the local level of the void space. Furthermore, at high values of Re, the nonlinear advection term in the Navier-Stokes equations become relevant and can lead to vortices and flow separation. Indeed, in their numerical simulations of flows through closed-packed spheres in a fcc arrangement with the gradient in applied pressure oriented along the [001] direction, Hill and Koch [3] observed that with increasing Reynolds number, the

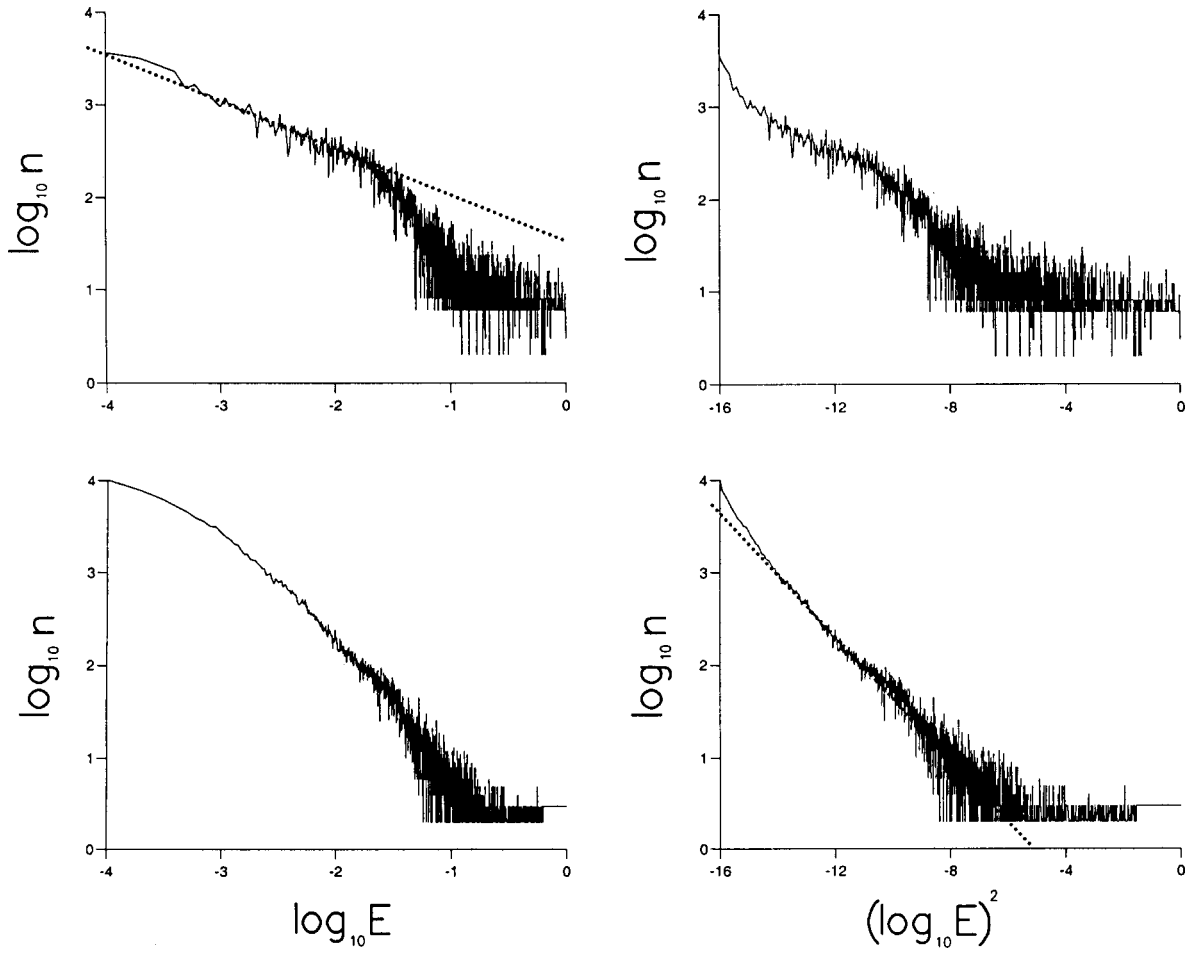

FIG. 2. The distribution of normalized local kinetic energy for a steady flow with Re≈0.2 (top) and a chaotic flow with Re≈19.8 (bottom). The power-law scaling regimes are indicated by dashed lines.

geometrical structure of the flow changes from one that is dominated by extension and shear to one in which the trajectories are helical. That is, with increasing Re, velocity and vorticity, $\boldsymbol{\omega}=\nabla\times\mathbf{u}$, become more closely aligned.

C. Helicity

The distributions of $\cos\varphi=\mathbf{u}\cdot\boldsymbol{\omega}/|\mathbf{u}||\boldsymbol{\omega}|$ shown in Fig. 3 demonstrate such transitions also occur for the period-1, -2, and -3 arrangements. For all three arrangements, there is,

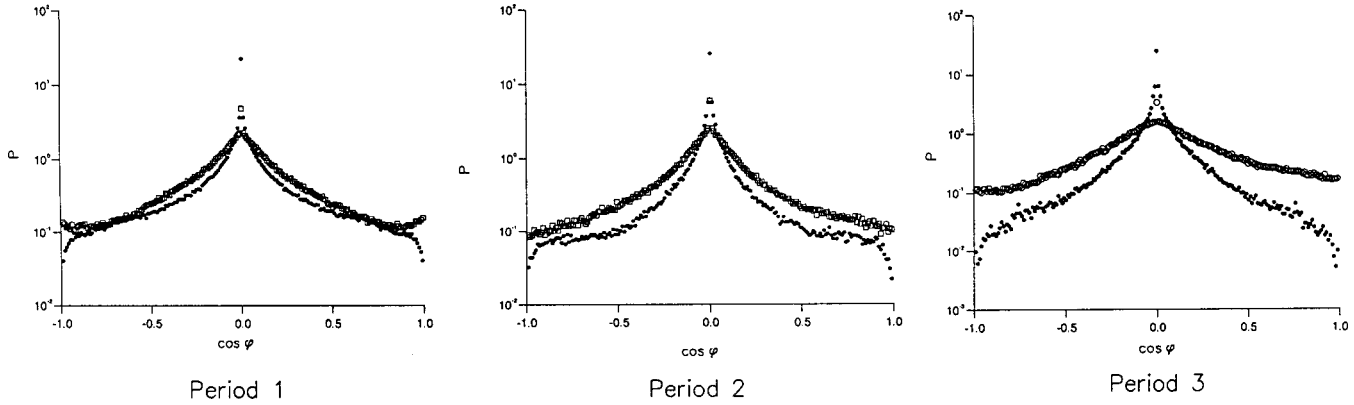

FIG. 3. The probability density function of the cosine of the angle between the velocity and the vorticity at a single instant in time for the period 1 (left: ●, steady flow with Re≈50.6; □, chaotic flow with Re≈379.4), period 2, (middle: ●, steady flow with Re≈0.2; □, chaotic flow with Re≈19.8; distributions for Re≈19.8 and 650 were not found to be significantly different) and the period 3 (right: ●, steady flow with Re≈0.2; ○, chaotic flow with Re≈113; distributions for Re≈113 and 2200 were not found to be significantly different) arrangement of spheres.

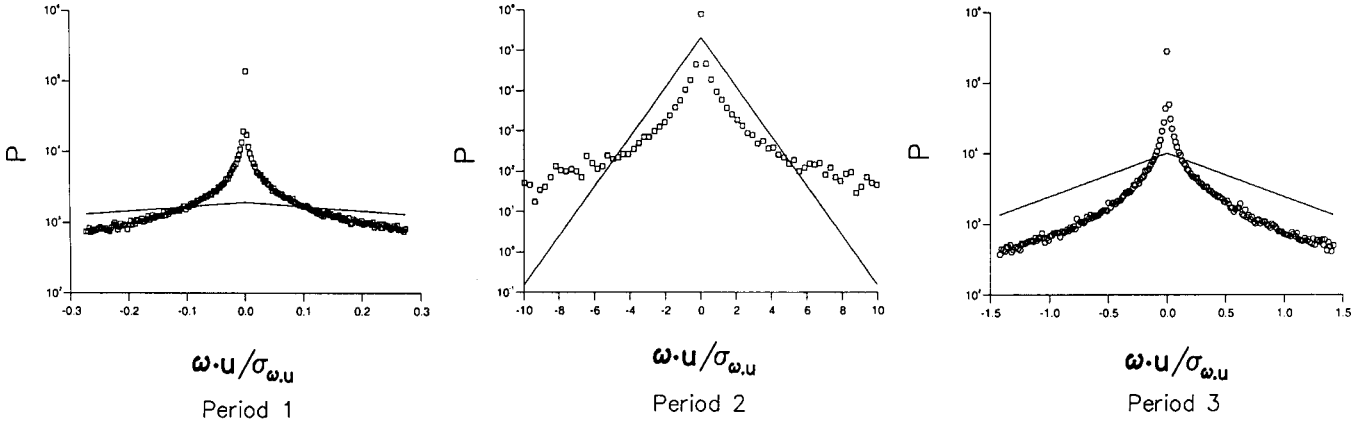

FIG. 4. The probability density function, at a single instant in time of helicity for turbulent flows through the period 1 (left, Re $\approx$379.4), 2 (middle, Re$\approx$19.8; a similar distribution was obtained for Re$\approx$650) and 3 (right, Re$\approx$113) arrangement of spheres. The lines are double exponential distributions with zero mean and standard deviation $\sigma_{\omega \cdot \mathbf{u}}$.

with increasing Reynolds number, a decrease in the magnitude of the peak of the distribution at $\cos\varphi=0$, caused by fluid in the outer regions penetrating into the shear-dominated flow close to the spheres and an increase in the tail of the distribution at $\cos\varphi=\pm 1$ caused by the closer alignment of velocity and vorticity. These findings suggest that the mechanism proposed by Hill and Koch [3] for the transfer of energy to smaller scales by the dynamic interaction of vortices is generally applicable to flows through arbitrary closely packed arrangements of spheres (irrespective of whether changes in geometry are brought about the packing arrangement or by a reorientation of the gradient in applied pressure) and that the occurrence of helical trajectories is a generic feature of such turbulent flows. The later has important implications for particle transport because helicity, even when time dependent, is an important quantity governing dispersion and is associated with suppressed rates of turbulent dispersion at long times and anomalous dispersion at intermediate times [25,26]. Note, however, that within the channels in the period-1 and -2 arrangements, the probability of $|\cos\varphi|>0.5$ is negligibly small when $\mathrm{Re}<O(10^3)$.

The distributions of helicity $\mathbf{h}=\mathbf{u}\cdot\boldsymbol{\omega}$ in moderate Reynolds-number [$\mathrm{Re}\sim O(10^2)$] turbulent flows are, however, strongly dependent upon geometry. For the period-3 arrangement with the gradient in applied pressure in the [001] direction, this distribution is close to being a double exponential [3], while for the period-1, -2, and -3 arrangements considered here it is not, as demonstrated in Fig. 4. For these arrangements, a double exponential distribution only arises when $\mathrm{Re}>O(10^2)$, as illustrated in Fig. 5.

D. Channelling

A key difference between the fcc and the period-1 and -2 arrangements of spheres is the orientation of straight channels through the packed bed. For the period-1 and -2 arrangement these channels are oriented along the [001] direction, which is the most natural orientation of the gradient in applied pressure and the orientation adopted in the present study. As shown in Fig. 6, for the period-2 arrangement of spheres, channelling occurs when the flow is steady but breakdowns at moderate Reynolds numbers when the magnitude and orientation of the quasiperiodic flow within the channels becomes subject to large spatial-temporal fluctuations, which lead to a destabilizing the flow throughout the bed. Channelling is seen to re-emerge at such larger Reynolds numbers when the flow becomes turbulent.

Tracer particles released from sources located within channels and into the quasiperiodic flow were found to disperse throughout the bed, while the majority of those released into the turbulent flow (and advected by the resolved fluid motions) were found to remain within the channels. The re-emergence of channelling at high-Reynolds numbers can, therefore, be expected to be accompanied by a reduction in diffusivity. Tracer particle in the quasiperiodic flow is examined in more detail in the next section.

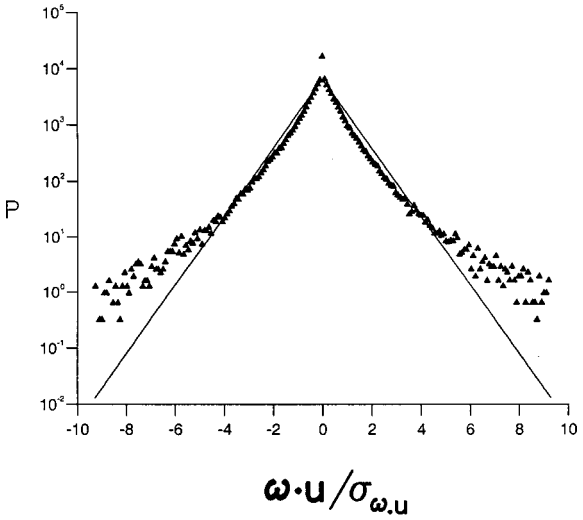

FIG. 5. The probability density function, at a single instant in time, of the helicity from the lattice Boltzmann simulations for a chaotic flow Re$\approx$2200 through closed-packed spheres in a fcc arrangement with the gradient in applied pressure in the [111] direction. The lines are double exponential distributions with zero mean and standard deviation $\sigma_{\omega \cdot \mathbf{u}}$.

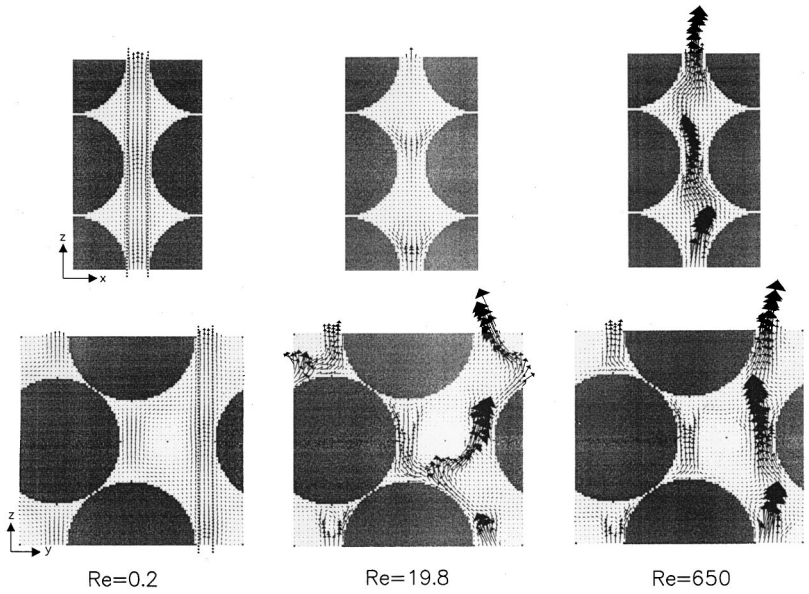

FIG. 6. Snap shots of the predicted velocity components in the *x*-*z* and *y*-*z* planes passing through the middle of the channel (indicated by the dashed line) of the period-2 arrangement of spheres for a steady flow with Re≈0.2, a quasiperiodic flow with Re≈19.8 and a turbulent flow with Re≈650. For clarity, only every second vector is plotted. A vector with length equal to a sphere radius corresponds to a projected speed $|\mathbf{u}|=0.06$, nondimensionalized on the sphere radius and the kinematic viscosity. To remove the ''staggered momentum,'' velocity components have been averaged over two successive interactions *n* of the lattice Boltzmann equation.

E. Dispersion characteristics

In the absence of molecular diffusion, dispersion in steady flows can only arise from distributed sources through the action of mean-streamline straining (i.e., convective dispersion). This mechanism is likely to be most effective when the gradient in applied pressure is not aligned with a principal axis or when the Eulerian flow is unsteady because then particle trajectories can be nonperiodic. As for the fcc arrangement of spheres [1], the root-mean-square spread of tracer-particles σ at a distance d from a point source in the quasiperiodic flow with the hcp arrangement of spheres is seen in Fig. 7 to obey $\sigma \propto d^{1/2}$ in the far field. The observed anisotropy arises because the source, which is located within a void that is not in channel, is approximately one sphere radius from the nearest channel in the *y* direction but is approximately $\sqrt{3}$ radii from the nearest channel in the *x* direction. The corresponding temporal development of dispersion is shown in Fig. 8. Transport is seen to be ballistic at short times and Fickian in the far field, while at intermediate times, it is superdiffusive and faster than ballistic. The Fickian dispersion characteristic is most probably a consequence of the length and time scales on which transport occurs being much longer than the scales on which the velocity field experienced by the particles varies.

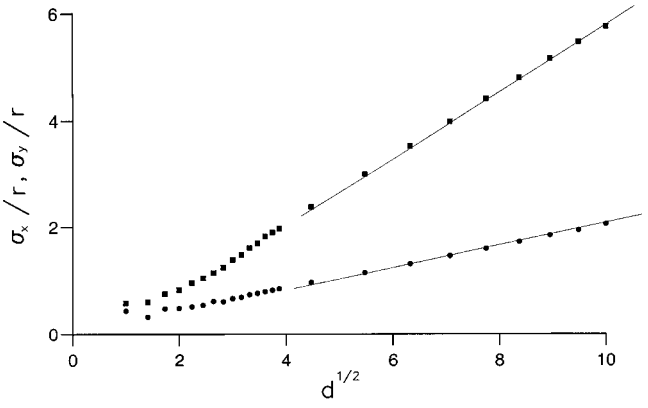

FIG. 7. The predicted rms spread of tracer-particles σ_x and σ_y (*x* direction, ●; *y* direction ■) from a continuous point source within a void (not in a channel) into the quasiperiodic flow with Re≈19.8 and within the period-2 arrangement of spheres, as a function of $(d)^{1/2}$, where *d* is the distance from the source measured in sphere diameters. The power-law regimes are indicated by solid lines.

Intermediate-time superdiffusion occurs for displacements between about 0.7 and 2.8 sphere radii in the direction of the gradient in applied pressure, which corresponds to transport around the first and second spheres encountered by the tracer particles, and consequently, to the first and second encounters tracer particles have with stagnation points in the flow. The extent and degree of the superdiffusion is seen to be more pronounced in the simulation data for the period-2 than for the period-3 arrangement and in both cases increases with increasing Reynolds number. Indeed, the simulation data for the hcp arrangement clearly shows the emergence of anomalous power-law dispersion, which for $\mathrm{Re}\sim O(10^3)$ extends over about one order of magnitude in nondimensional times, $t/(r^2/v)$. The possibility but not the superdiffusive characteristic *per se* of such rapid plume growth in the vicinity of a ''stagnation streamline'' and around an obstacle in a turbulent flow has been investigated previously using a generalization of rapid distortion theory [7,8]. According to this theory, dispersion is enhanced by mean-streamline straining.

For the period-3 packing arrangement, the transition from superdiffusion to Fickian dispersion is seen in Fig. 8 to be distinguished by a regime of subdiffusion. This subdiffusion may be a consequence of particle entrapment in the viscous boundary layers close to the solid surfaces and the contraction of mean streamlines in the ''wake'' flows behind the spheres [7,8]. For the hcp arrangement of spheres, these subdiffusive effects are probably masked by the dominance of superdiffusion. Support for this conjecture comes from the simulation data for a source located within a direct channel and far from a stagnation streamline which, as shown in Fig. 8, exhibits subdiffusion at intermediate times.

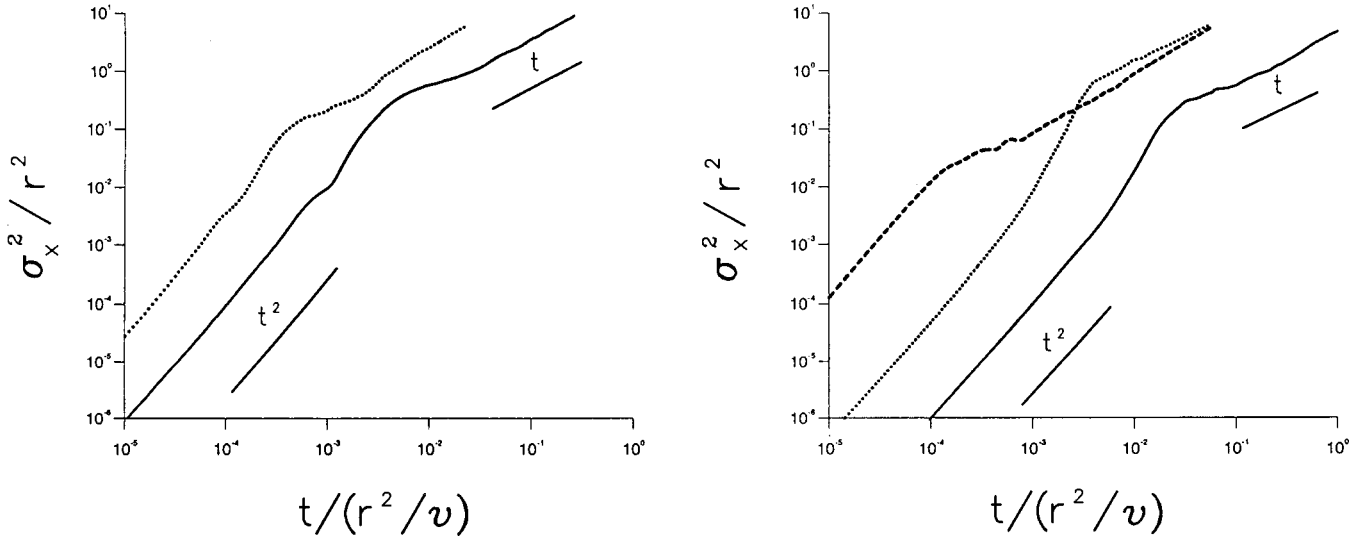

FIG. 8. The predicted mean-square spread of tracer-particles σ_x^2, from a source on the ''stagnation streamline'' in directions normal to the gradient in applied pressure as a function of time, t for the fcc (left) and hcp (right) arrangements of spheres. Predictions are shown for flows within the hcp arrangement of spheres with $\mathrm{Re}\sim O(10^2)$ (solid lines) and $\mathrm{Re}\sim O(10^3)$ (dotted lines). Also shown (dashed line) are predictions for the dispersion of tracer particles from a source located within an open channel into a flow with $\mathrm{Re}\sim O(10^3)$. The regimes of ballistic ($\sigma_x^2 \propto t^2$) and Fickian ($\sigma_x \propto t$) transport are indicated. Quantities have been rendered nondimensional using the sphere radius r and the viscosity ν. At times $t/(r^2/\nu)\sim O(10^3)$, tracer particles have typically traversed a distance greater than $20r$.

IV. CONCLUSIONS

In this paper, flow and dispersion through a fixed bed of spheres in a period-1, period-2 (hcp), and period-3 (fcc) arrangement of spheres have been studied in numerical simulations. For the period-1, -2 and -3 packing arrangements, there is a transition with increasing Reynolds number from a power-law to a log-normal distribution of turbulent kinetic energies and, velocity and vorticity become more closely aligned. The power-law distribution of turbulent kinetic energies indicates that the ''stagnant'' zones of steady flows play a significant role in determining transport, contrary to the dangling bonds in the analogous electrical transport problem, while the occurrence of helical trajectories has important consequences for turbulent transport processes, resulting in suppressed rates of turbulent dispersion at long times and anomalous dispersion at intermediate times [25,26]. The robustness of these flow and dispersion characteristics to changes in periodicity suggests that they persist when the packing geometry is effectively changed by a reorientation of the direction of the gradient in applied pressure. This conjecture is supported by simulation data for the fcc close-packing arrangement with the gradient in applied pressure oriented along the [111] and [001] directions [1–3].

For steady and strongly turbulent flows, the channels through the period-1 and -2 arrangements of spheres provide direct routes for marked fluid-particle transport but for weakly turbulent flows influence dispersion primarily by destabilizing the flow throughout the entire flow domain.

ACKNOWLEDGMENTS

This work was partly supported by the BBSRC through ROPA Grant No. 978945. I thank Reghan Hill of Princeton University for disclosing his unpublished findings and for fruitful communications.

[1] A. M. Reynolds, S. V. Reavell, and B. B. Harral, Phys. Rev. E **62**, 3632 (2000).
[2] R. J. Hill and D. L. Koch, Bull. Am. Phys. Soc. **44**, 69 (1999).
[3] R. J. Hill and D. L. Koch, J. Fluid Mech. (to be published).
[4] D. L. Koch and A. J. C. Ladd, J. Fluid Mech. **349**, 31 (1997).
[5] D. Koch and J. F. Brady, J. Fluid Mech. **154**, 399 (1985).
[6] L. Borland, Phys. Rev. E **57**, 6634 (1998).
[7] J. C. R. Hunt and P. J. Mulhearn, J. Fluid Mech. **61**, 245 (1973).
[8] J. C. R. Hunt, J. Fluid Mech. **61**, 625 (1973).
[9] D. Elhmaïdi, A. Provenzale, and A. Babiano, J. Fluid Mech. **257**, 533 (1993).
[10] A. R. Osborne, A. D. Kirwan, A. Provenzale, and L. Bergamasco, Tellus, Ser. A **41**, 416 (1989).
[11] B. G. Sanderson, A. Goulding, and A. Okubu, Tellus, Ser. A **43**, 550 (1990).
[12] B. G. Sanderson and D. A. Booth, Tellus, Ser. A **43**, 334 (1991).
[13] A. Provenzale, A. R. Osborne, A. D. Kirwan, and L. Bergamasco, in *Nonlinear Topics in Ocean Physics*, edited by A. R. Osborne (Elsevier, New York, 1991), pp. 367–401.
[14] Y. H. Qian, D. d'Humieres, and P. Lallemand, Europhys. Lett. **17**, 479 (1992).
[15] S. Chen and G. D. Doolen, Annu. Rev. Fluid Mech. **30**, 329 (1998).
[16] I. Ginzbourg and P. M. Adler, J. Phys. II **4**, 191 (1994).

[17] D. R. Noble, S. Y. Chen, J. G. Georgiadis, and R. O. Buckius, Phys. Fluids **7**, 203 (1995).
[18] R. Verberg and A. J. C. Ladd, Phys. Rev. Lett. **84**, 2148 (2000).
[19] S. Hou, J. Sterling, S. Chen, and G. D. Doolen, Fields Institute Communications **6**, 151 (1996).
[20] J. M. Buick and C. A. Greated, Phys. Rev. E **61**, 5307 (2000); J. M. Buick, Ph.D thesis, University of Edinburgh, UK, 1997.
[21] D. Kandhai, A. Koponen, A. Heokstra, M. Kataja, J. Timonen, and P. M. A. Sloot, J. Comp. Physiol. **150**, 482 (1999).
[22] L. de Arcangelis, S. Redner, and A. Coniglio, Phys. Rev. B **31**, 4725 (1985).
[23] L. de Arcangelis, S. Redner, and A. Coniglio, Phys. Rev. B **34**, 4656 (1986).
[24] J. S. Andrade Jr., M. P. Almeida, J. Mendes Filho, S. Havlin, B. Suki, and H. E. Stanley, Phys. Rev. Lett. **20**, 3901 (1997).
[25] M. S. Borgas, T. K. Flesch, and B. L. Sawford, J. Fluid Mech. **332**, 141 (1997).
[26] A. M. Reynolds, Boundary-Layer Meteorology (to be published).